Optics Communications 363 (2016) 85–90

Contents lists available at ScienceDirect

Optics Communications

journal homepage: www.elsevier.com/locate/optcom

Arrays of Gaussian vortex, Bessel and Airy beams by computer-generated hologram

Yang Lu [a], Bo Jiang [a], Shuchao Lü [a], Yongqi Liu [a], Shasha Li [a], Zheng Cao [a,b], Xinyuan Qi [a,*]

[a] School of Physics, Northwest University, No. 229, Taibai North Road, Xi'an, Shaanxi 710069, China
[b] National Key Laboratory of Science and Technology on Space Microwave, CAST, Xi'an, Shaanxi 710100, China

ARTICLE INFO

Article history:
Received 19 August 2015
Received in revised form
28 October 2015
Accepted 1 November 2015
Available online 12 November 2015

Keywords:
Spatial light modulator
Fractional-Talbot effect
Rayleigh length
Photonic lattice

ABSTRACT

We generate various kinds of arrays of Gaussian vortex, Bessel and Airy beams, respectively, with digital phase holograms (DPH) based on the fractional-Talbot effect by using the phase-only spatial light modulator (SLM). The linear and nonlinear transmissions of these beam arrays in strontium barium niobate (SBN) crystal are investigated numerically and experimentally. Compared with Gaussian vortex arrays, Bessel and Airy beam arrays can keep their patterns unchanged in over 20 mm, realizing non-diffracting transmission. The Fourier spectra (far-field diffraction patterns) of the lattices are also studied. The experimental results are in good agreement with the numerical simulations.

1. Introduction

Optical vortex, Bessel and Airy beams are special light fields, widely studied and employed in the fields of particle trapping and sorting [1–4], quantum optics [5], optical communications [6], optical computation [7], optical fiber applications [8], curved plasmon channel generation [9,10] and etc. Optical vortex [6] following the phase singularity along the axis of a beam with helical phase fronts characterized by $\exp(il\theta)$. Bessel beams, a kind of non-diffracting light beams, were proposed by Durnin in the late 1980s [11], which have an infinite number of rings covering an infinite distance and requiring an infinite amount of power [12]. Recent works have showed that Bessel-like beam patterns can be delivered along sinusoidal [13] and even self-accelerating along predesigned trajectories [14]. Airy beams, another type of non-diffracting beams, have attracted much interest since 2007 due to the unique properties of self-accelerating and self-healing, when Siviloglou and et al. firstly reported in the field of optics [15,16]. For the particularity of these special beams, people pay close attention not only to these beams themselves, but also to these beam arrays. Arrays always have more fascinating characteristics and more practical applications. There are many ways to generate beam arrays such as multi-beam interference [17,18], Dammann grating [19], etc. The application domains of these methods are limited either because of the simple structures of the beam arrays or because of the expensive costs of the devices. Talbot effect [20,21] can also be used to generate periodic and complicated structures of arrays when a periodic object is illuminated with a coherent light wave. The light distribution at the fractional-Talbot distance has also been shown to produce image-like patterns [2,22]. Compared with the images in the integer Talbot effect, the recurring patterns will be smaller but with higher light intensity in the fractional-Talbot effect.

In this paper, we focus on the fractional-Talbot effect to generate diversified structures of arrays of Gaussian vortex, Bessel and Airy beams, and study the linear and nonlinear transmissions of these beam arrays in the SBN crystal numerically and experimentally.

2. Theoretical analysis

The complex optical field of the beam arrays $U_0(\boldsymbol{r})$ can be described by a function as follows

$$U_0(\boldsymbol{r}) = u_0(\boldsymbol{r}) \otimes lattice(\boldsymbol{r}, \boldsymbol{R_n}) \tag{1}$$

where $\otimes$ denotes the convolution integral, $u_0(\boldsymbol{r})$ is the complex amplitude of one cell in the array, $\boldsymbol{r}$ is the position vector, and $lattice(\boldsymbol{r}, \boldsymbol{R}_n)$ defines an array of the two-dimensional (2D) period δ function with the lattice vector of $\boldsymbol{R}_n = n_1\boldsymbol{a}_1 + n_2\boldsymbol{a}_2$ (here n_1 and n_2 are the lattice index, and $\boldsymbol{a}_1$ and $\boldsymbol{a}_2$ are the basis vectors of the lattice). The functions $lattice(\boldsymbol{r}, \boldsymbol{R}_n)$ of three different arrays with rectangular, diamond and hexagon symmetries obey

* Corresponding author.
E-mail address: qixycn@nwu.edu.cn (X. Qi).

http://dx.doi.org/10.1016/j.optcom.2015.11.001
0030-4018/

$$\begin{cases} lattice_{\mathrm{Rec}} = comb\left(\dfrac{x}{a_1}, \dfrac{y}{a_2}\right) & \\ lattice_{Dia} = comb\left(\dfrac{x}{a_1}, \dfrac{y}{a_2}\right) & (a_1 = a_2) \\ \qquad + comb\left(\dfrac{x}{a_1} + \dfrac{1}{2}, \dfrac{y}{a_2} + \dfrac{1}{2}\right) & \\ lattice_{Hex} = comb\left(\dfrac{x}{a_1}, \dfrac{y}{a_2}\right) & \left(a_1 = \dfrac{\sqrt{3}}{3} a_2\right) \\ \qquad + comb\left(\dfrac{x}{a_1} + \dfrac{1}{2}, \dfrac{y}{a_2} + \dfrac{1}{2}\right) & \end{cases} \tag{2}$$

Based on the fractional-Talbot effect, the phase distribution Φ of the complex field $U_0(\boldsymbol{r})$ is employed as the pure phase mask to recover $U_0(\boldsymbol{r})$ [2]. Φ can be calculated by the convolution of the cell phase ϕ and the $lattice(\boldsymbol{r}, \boldsymbol{R}_n)$. The field pattern $U_0(\boldsymbol{r})$ recurs at $z = z_T/\beta$, where β is an integer. $z_T = 2d^2/\lambda$ is the Talbot distance [21], d is the period of the optical phase grating and λ is the wavelength of a light beam.

3. Experimental setup

Experiment confirmation of the above analysis is performed by using a 532 nm laser beam projected onto a $5 \times 5 \times 10$ mm^3 SBN crystal. The setup is shown in Fig. 1. The creation of the arrays consists of six basic steps: (1) after laser expansion by the lenses L_1 and L_2, an initial Gaussian beam turns out to be a quasi-plane wave, launching onto a SLM, then (2) different kinds phase patterns (DPHs), which are computer calculated by the phase of the complex light field $U_0(\boldsymbol{r})$, are impressed upon the beam and corresponding lattice patterns recover at the fractional-Talbot plane (the black frame), (3) a 4f system (L_3 and L_4) and a filter are used to obtain only the first order diffraction pattern of the DPHs, (4) through changing different positions of the lens L_5, the arrays at different fractional-Talbot distances are imaged onto the front facet of the SBN crystal, (5) the lens L_6 and CCD_1 are used to observe the intensity patterns of beam arrays, and (6) the lens L_7 and CCD_2 are needed to monitor the Fourier spectra of different arrays at the rear focal plane of the lens L_6. The red line in Fig. 1 shows Rayleigh length L_{ci} during which the beam keeps almost invariant.

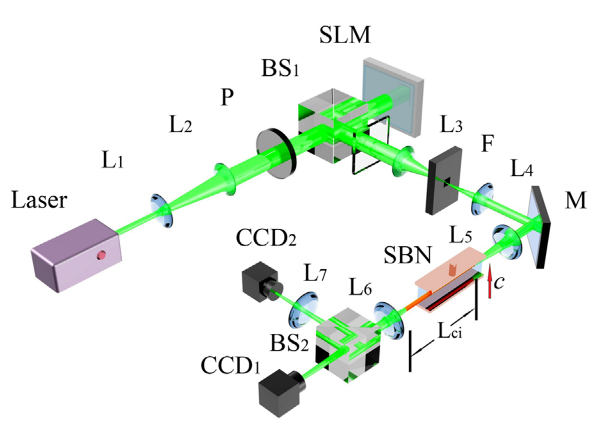

Fig. 1. The sketch of the experimental setup. L, Fourier transform lens; P, polarizer; BS, beam splitter; SLM, spatial light modulator; F, filter; M, mirror; SBN, strontium barium niobate crystal; c, crystal axis; CCD, charge coupled device; L_{ci}, Rayleigh length of a beam; black frame, fractional-Talbot plane.

4. Numerical simulations and experimental results

4.1. Simple arrays

First, we studied some simple arrays of Gaussian vortex, Bessel and Airy beams. Typical numerical and experimental results are shown in Fig. 2. From the left column in Fig. 2, we can see vortex arrays (topological charge l=3) arranged in common rectangular shape. Due to the finite size of a Gaussian vortex beam, it is used as the cell of the vortex beam array. The cell phase ϕ_{Gv} is shown in Fig. 2(a1) upper right, which consists of ϕ_G (the phase of a Gaussian beam) and ϕ_v (the phase of a vortex beam), $\phi_{Gv} = \phi_v \cdot \phi_G = \exp\{i[l\theta - r^2/2R]\}$, here l topological charges, θ the angular coordinate in the polar coordinate system, r the radial coordinate in the polar coordinate system, R constant. Analogously, the cell phase of a Bessel beam array follows $\phi_{Bes}(r) = mr$ [23], where $m = (\eta - 1)\alpha/k_0$, η refractive index of a circularly symmetric glass cone, α exterior-angle, $k_0 = 2\pi/\lambda$ wavevector, and r the radial coordinate in the polar coordinate system [Fig. 2(b1)]. The cell phase of an Airy beam array can be approximated quite well by [16] [Fig. 2(c1)], $\phi_{Ai}(x, z = 0) \approx x^{-1/4} \exp[iCx^{3/2}]$, where C is a constant, x, z are the transverse and longitudinal coordinates, respectively.

The pattern on the fractional-Talbot plane, which is $z_T/\beta \approx 36.7$ cm ($\beta = 17$) away from SLM, is projected by the lens L_5 on the input face of the SBN crystal precisely. The arrays are shown in Fig. 2(a4–c4). The periods of the input arrays of Gaussian vortex and Bessel are roughly $\Lambda \approx 300$ μm, while the Airy arrays' period is about $\Lambda \approx 450$ μm at z=0 to make sure the side lobes and tail lobes clear enough (the period of side lobes is around 20 μm). The simulated and experimental light profiles of three beam arrays in one period are both plotted in Fig. 2 (a5–c5). Obviously, the results fit pretty well, exhibiting excellent optical quality of the beam arrays.

4.2. Linear and nonlinear transmissions

Based on the aforementioned studies, we further investigated the linear and nonlinear transmissions of beam arrays $U_{defect}(\boldsymbol{r})$ with a site defect by introducing a δ function in the $lattice(\boldsymbol{r}, \boldsymbol{R}_n)$ in homogeneous medium, $U_{defect}(\boldsymbol{r}) = u_0(\boldsymbol{r}) \otimes [lattice(\boldsymbol{r}, \boldsymbol{R}_n) - \delta_{\boldsymbol{R}_n}]$. The recurring patterns on the input facet of the SBN crystal are shown in Fig. 3(a1–c1). The periods of Gaussian vortex and Bessel arrays are both about $\Lambda \approx 130$ μm, while the Airy array still keeps $\Lambda \approx 450$ μm (at z=0). Fig. 3(a2–c2) shows the linear output patterns of the arrays propagating 10 mm through the SBN crystal. Obviously, the cells in the diamond Gaussian vortex array distort to a certain extent, whereas the cells in the hexagon Bessel beam array and the rectangular Airy beam array maintain almost unchanged. This is because these three kinds of cells have different Rayleigh lengths L_{ci} during the same fractional-Talbot distance. The recurring image distorts gradually from one fractional-Talbot plane to maximum extent and then evolves into another recurring image until the next fractional-Talbot plane [24]. The Rayleigh length of a Gaussian vortex beam L_{cV} is measured about 3 mm (shorter than the length of the crystal 10 mm), while the Rayleigh lengths of Bessel and Airy beams are longer than 20 mm, which means that they can keep their shapes in the whole crystal. In the nonlinear case, the biased field applied along the c-axis of the SBN crystal was 800 V/cm. Under the self-focusing nonlinearity, the patterns on the output [Fig. 3(a3–c3)] shrink, compared with the linear output patterns shown in Fig. 3(a2–c2). The sizes and shapes of the Bessel beam array and the Airy beam array [Fig. 3(b3 and c3)] keep nearly unchanged, compared with the input patterns [Fig. 3(b1 and c1)]. However, the Gaussian vortex array cannot recover to its input pattern even with the same biased field